Construction and Building Materials 301 (2021) 124078

Contents lists available at ScienceDirect

Construction and Building Materials

journal homepage: www.elsevier.com/locate/conbuildmat

Enhanced adhesive performance of epoxy resin coating by a novel bonding agent

Łukasz Sadowski [a,*], Łukasz Kampa [a], Agnieszka Chowaniec [a], Aleksandra Królicka [b], Andrzej Żak [c], Hassan Abdoulpour [a], Sabrina Vantadori [d]

[a] Department of Building Engineering, Wroclaw University of Science and Technology, Wybrzeże Wyspiańskiego 27, 50-370 Wroclaw, Poland
[b] Department of Metal Forming, Welding and Metrology, Wroclaw University of Science and Technology, Wybrzeże Wyspiańskiego 27, 50-370 Wroclaw, Poland
[c] Electron Microscopy Laboratory, Faculty of Mechanical Engineering, Wroclaw University of Science and Technology, Wybrzeże Wyspiańskiego 27, 50-370 Wrocław, Poland
[d] Department of Engineering & Architecture, University of Parma, Parco Area delle Scienze 181/A, 43124 Parma, Italy

HIGHLIGHTS

- The novel epoxy resin bonding agent was proposed.
- The bonding agent improves the bonding strength of epoxy resin coatings.
- The bonding agent was modified with the addition of coconut fibers.
- The addition of 0.5% of coconut fibers to the bonding agent was beneficial.
- The interface between the coating and substrate was analyzed.

GRAPHICAL ABSTRACT

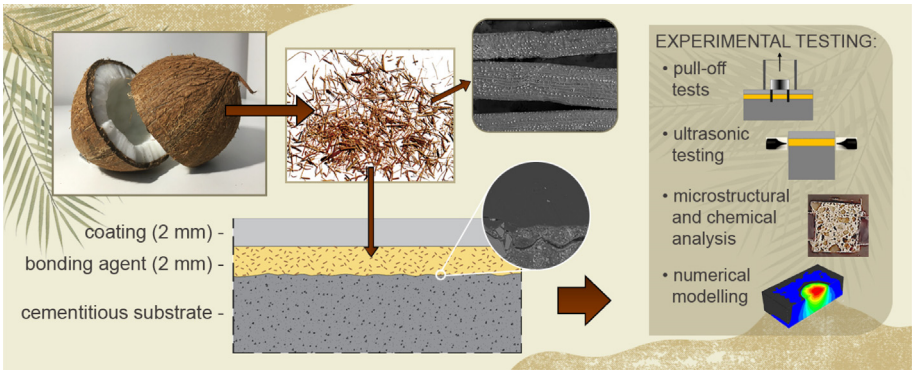

ARTICLE INFO

Article history:
Received 28 April 2021
Received in revised form 21 June 2021
Accepted 22 June 2021

Keywords:
Cementitious substrate
Bonding agent
Coating
Epoxy resin
Pull-off strength
Adhesion

ABSTRACT

The current paper aims to propose a novel epoxy resin bonding agent for improving the bonding strength of epoxy resin coating systems. These kinds of systems are mainly employed during the repair and maintenance of existing cement-based structures, especially concrete floors. The paper presents the results of a series of tests of epoxy resin coatings, in which the matrix of the bonding agent made of epoxy resin is modified with the addition of coconut fibers. Pull-off strength tests were performed on the cement paste and cement mortar substrates. The results presented that the addition of 0.5%-1.0% of coconut fibers to the bonding agent matrix resulted in increased pull-off strength of the coating. In turn, it was observed that in the case of using a higher volume fraction of fibers the occurrence for the delamination failure between the epoxy resin and substrate was more pronounced. This is manifested by the reduction of the pull-off strength of the epoxy resin coating and is probably caused by the increased presence of fiber clusters in the epoxy resin matrix. Finally, to confirm the obtained macroscopic results, the specimens were analyzed using the scanning electron microscopy method by examining the interface between the coating and substrate. Numerical simulations were successfully predicting the behavior of pull-off strength using simplified concrete damage plasticity. The linear behavior was defined for presenting the softening behavior of the substrate during loading.

* Corresponding author.
E-mail address: lukasz.sadowski@pwr.edu.pl (Ł. Sadowski).

https://doi.org/10.1016/j.conbuildmat.2021.124078
0950-0618/

1. Introduction

Cement-based materials are commonly used to build reinforced concrete structures on land and water [1]. In aggressive environmental conditions where the structures are exposed to degradations, providing some protection layers can effectively increase the service life of the structures [2].

The protection methods that are commonly used include: (i) the use of protective coatings on cement-based surface protective coating, (ii) rebars coating and (iii) corrosion inhibitors [3–9]. Some of these methods are suitable for new concrete structures, whereas others may also be adopted for existing structures (e.g., in repairs [10–15]).

There are existing various types of coating protectives ranging from simple to complex formulations and materialized by inorganic and/or organic constituents. These coating protectives are efficient for enhancing cementitious materials durability performances. Moreover, studies to date have shown encouraging results on their performance [16–19].

The bonding strength between the coating and the absorptive substrates is an important indicator for measuring the service performance of a coating system [20–23]. Therefore, the bonding mechanism within the interface between the coating and the substrate has been a fundamental and important subject of research in the field of surface engineering [24–27].

Considering a coating system that consists of an epoxy resin coating placed on a cementitious substrate. Before the application of the coating, this substrate is covered and strengthened with an epoxy resin bonding agent. Such a coating type is widely used in existing concrete elements, such as floors, to strengthen the near-surface zone of existing cementitious substrates and to avoid their demolition and rebuilding. More precisely, the concrete floor is first ground and cleaned, then the bonding agent is applied, and the final finishing epoxy resin is placed.

To increase the pull-off strength of the aforementioned system [28], three strategies can be adopted as: (a) the coating's composition, (b) the cement substrate's composition, and (c) the bonding agent's composition.

In the context of point (a), regarding the modification of a coating's composition, recent investigations have shown that the addition of both glass powder [29,30] and glass fibers [31] improves the selected adhesive properties of epoxy resin coatings. Afshar et al., [32] studied the possibility of decreasing the corrosion rate in reinforced concrete and consequently increasing the durability of concrete structures. Different concrete additives and coatings on rebars were proposed. It was demonstrated that the polyurethane coating had the highest strength and the lowest corrosion compared to the other proposed coatings in that research.. De la Varga et al., [33] obtained a high pull-off strength by modifying the coatings with nanosilica. In turn, Morshed et al., [34] used nanosilica together with carbon nanotubes as additives to epoxy resin and observed a favourable effect on the bonding between the polymer composites and substrate. Pourhashema et al., [35] investigated the effect of hybrid SiO_2-graphene oxide added to the resin and found that the corrosion resistance of the coating, the adhesion, and water contact angle of the epoxy coating were significantly increased. It is worth noting that one method to enhance the pull-off strength, which does not require surface treatment, is the use of monomers, polymers, and nanomaterials [36–38].

In the context of point (b), the modification of a substrate's composition aims to increase the surface morphology of the substrate. This was recently proved by Van Der Putten et al., [39], who modified the composition of the substrate's near surface zone by adding both a comb (equipped with 34 small needles placed next to each other) and sand.

In the context of point (c), regarding the modification of a bonding agent's composition, Kim et al., [40] proposed an aminosilane-modified resin-based bonding agent. Other modification attempts were made by adding polypropylene fibers [41]. It was observed that the addition of fibers in the cementitious substrate in an amount between 0.5 wt% and 1 wt% increased the pull-off strength with respect to specimens without fibers.

Vegetable fibers are relatively rarely used in building applications. Their use is confined to improve the physical and mechanical properties of cementitious substrates, rather than to enhance the bonding strength of coating systems [42–49]. As pointed out by Wei et al., [28], eco-friendly methods for improving the bond strength of epoxy-based industrial composite coatings are worth taking into consideration. As pointed out by Czarnecki and Van Gemert [50] environmentally-friendly innovations should be provided to solve the problem of the negative impact of the construction industry on the environment. According to Li et al., [51], vegetable fibers provide several advantages to composites when compared to synthetic fibers, such as biodegradability, low weight, low price, and satisfactory mechanical properties [52–54].

The novelty of the present paper is the proposal of a new epoxy resin bonding agent to improve the bonding strength of an epoxy resin coating system. The proposal involves the inclusion of coconut fibers in the bonding agent matrix.

Different cementitious substrates were examined: a cement paste and cement mortar. The coating was made of a commercial epoxy resin manufactured by Si-Tech (Jakubow, Poland). The bonding agent matrix, made of a commercial epoxy resin manufactured by Si-Tech (Jakubow, Poland), was modified with the addition of a different percent of coconut fibers (0.5%, 1.0%, 1.5% and 2.0% of the resin's weight). To the best of the authors' knowledge, it is worth noting that there are no attempts described in the literature to include vegetable fibers, and more precisely coconut fibers, in epoxy resin coating systems for improving their bonding strength.

The adhesive properties of such a novel coating system were experimentally investigated by carrying out pull-off tests. The microstructure of each used bonding agent was analysed with the use of scanning electron microscopy. In addition to that, finite element simulations were employed for further understanding regarding the bond strength and substrate failure. For this aim, ABAQUS software was utilized and the bond between substrate and coating was defined using cohesive elements and substrate failure model using Concrete Damage Plasticity (CDP). The reason for choosing the CDP model was due to high convergence, fewer analyses time, and less parameters essential for defining material behaviour.

2. Materials and preparation

2.1. Cementitious substrates

Two types of cementitious substrates were examined: cement paste and a cement mortar. The cement paste was composed of cement and water in a water-to-cement ratio equal to 0.4, whereas the cement mortar was made of cement, sand, and water in proportions of 1: 3: 0.5. The compressive strength of the cement paste was equal to 45.12 ± 0.90 MPa, whereas the flexural strength was equal to 4.65 ± 0.11 MPa. The compressive strength of the cement mortar was equal to 53.35 ± 1.08 MPa, whereas the flexural strength was equal to 5.12 ± 0.12 MPa.

Moulds with dimensions of 150 × 150 × 40 mm were used to prepare each of the above substrates. All dry ingredients were then

measured out and mixed in a mixer. After the dry ingredients were mixed, the water was added and mixed with a mixer arm for 90 s, followed by hand mixing for a further 90 s. The prepared mix was placed in the moulds, their surface was levelled, and they were then left for 24 h covered with plastic foil. After this time, the specimens were removed from the moulds and dried in air at 20–23 °C and 60–65% humidity for 28 days. After complete curing, the surface of the specimens was smoothed to an even surface.

2.2. The coating and the bonding agent

Commercial epoxy resins, which were obtained from bisphenol A and epichlorohydrin (number average molecular weight $\leq$ 700), were used for both the coating and the bonding agent matrix. For the coating, the commercial epoxy resin Meteor Stone, manufactured by Si-Tech (Jakubow, Poland) was used. The resin had a density of 1.15–1.25 g/cm^3, a viscosity of 750–1000 MPa·s, a shelf life (at 20 °C) of 20–25 min, and achieved full hardening after 24 h. For the bonding agent matrix, the commercial epoxy resin Meteor Primer, manufactured by Si-Tech (Jakubow, Poland) was used. It had a density of 1.0–1.2 g/cm^3 and a low viscosity of 400–600 MPa·s.

2.3. Coconut fibers

The view of the source of fibers, macrophotography of the coconut fibers is presented in Fig. 1**(a, b).** The fibers' diameter distribution was determined by randomly selecting 100 coconut fibers and employing both SEM images and ImageJ software (version 1.51w, National Institutes of Health, Bethesda, MA, USA [61]). Fig. 1**c** shows the obtained diameter distribution. The average diameter is equal to 258.9 ± 119.4 μm, whereas the median value is equal to 248.9 ± 55.0 μm. The fibers' length ranges from 8 to 10 mm. Such geometrical sizes are summarised in Table 1.

Moreover, the fibres' surface was characterized by expanded surface topography, as can be observed in Fig. 2**(a, b)**. They are characterized by a neutral pH, and their chemical composition, determined by the energy-dispersive X-ray spectroscopy method (EDS, EDX), is shown in Fig. 2**(c).** The dominance of carbon and the low fraction of oxygen can be observed in Fig. 2**(c)**. Moreover, from the observations of the fibers performed in the BSE (material contrast) mode (Fig. 2**(c)**), it was found that silicon dominated in the brighter regions.

2.4. Specimens of the coating system

The specimens for testing were derived from the specimens of the coating system. The specimens were prepared from the aforementioned cementitious substrates (see Section 2.1).

The epoxy resin, which was employed for the bonding agent (see Section 2.2), was mixed with the phenalkamine-based hardener in a ratio of 100 to 33. The coconut fibers (see Section 2.3) were added in a percentage of 0.5%, 1.0%, 1.5%, and 2.0% of the total weight of the resin. The mixture was then poured over the prepared substrates. A layer thickness of about 2 mm was obtained. The resin employed for the coating (see Section 2.2) was mixed with the phenalkamine-based hardener in a ratio of 100 to 50. The coating was then poured over the above layer, and a layer thickness of about 2 mm was obtained. It should be noted that there were protruding individual fibers and air bubbles observed on the top layer of some specimens. Therefore, to smooth the entire surface, the specimens were sanded using a grinder with a concrete grinding disc.

Moreover, to compare the results obtained with the use of the novel bonding agent, reference specimens were also prepared in which no fibers were added to the bonding agent. Fig. 3 shows the prepared specimens.

3. Experimental testing

3.1. Pull-off tests

The sample was divided into four regions, and therefore four tests could be performed on each specimen (Fig. 3**(a) and (b)**). The centre of each hole, according to the ASTM D4541-17 (Standard Test Method for Pull-Off Strength of Coatings Using Portable Adhesion Testers) standard for pull-off test [55]**,** was located at about 37 mm from the edge of the specimens. The holes were made using a diamond drill bit in concrete with an internal diameter of 5 cm and a rectangular shape of the teeth (Fig. 6). Drilling was performed at low speed - at the beginning of drilling, a device holding the drill was employed. The drill was cooled every few seconds during the drilling, but there was still a high temperature in the area of the drilled hole. After all boreholes were drilled, the top layer of each test specimen was cleaned of dust and washed with acetone to thoroughly clean and degrease. The pull-off tests were carried out according to the ASTM D4541-17 standard [55]

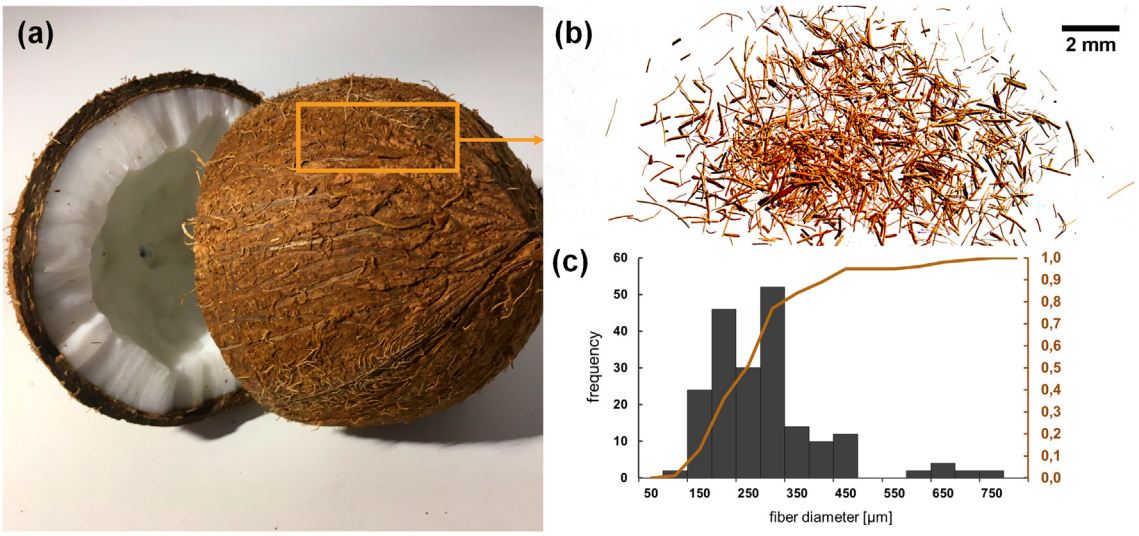

Fig. 1. Coconut fibers: (a) view of the source of fibers, (b) macrophotography, (c) diameter distribution.

Table 1
Characteristic sizes of the coconut fibers: mean value ($\overline{x}$), standard deviation (SD), first quartile (Q1), third quartile (Q3), interquartile range (IQR).

$\overline{x}$[μm]	SD [μm]	Median [μm]	Q1 [μm]	Q3 [μm]	$\frac{1}{2}$IQR [μm]
258.9	119.4	248.9	179.9	290.0	55.0

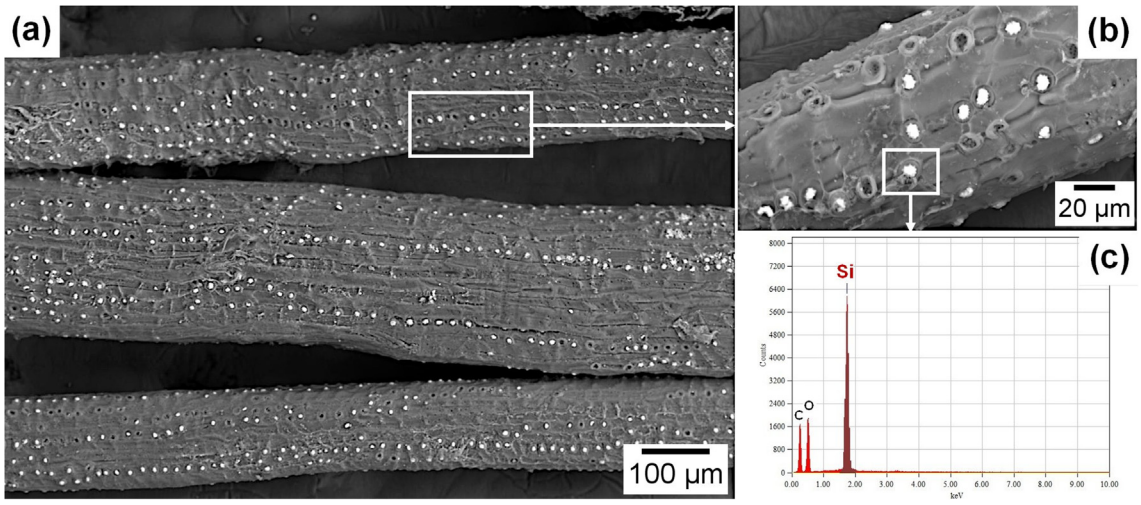

Fig. 2. Coconut fibers: (a, b) fiber surface image (SEM, BSE) used for chemical analysis, and (b) X-ray diffraction spectrum.

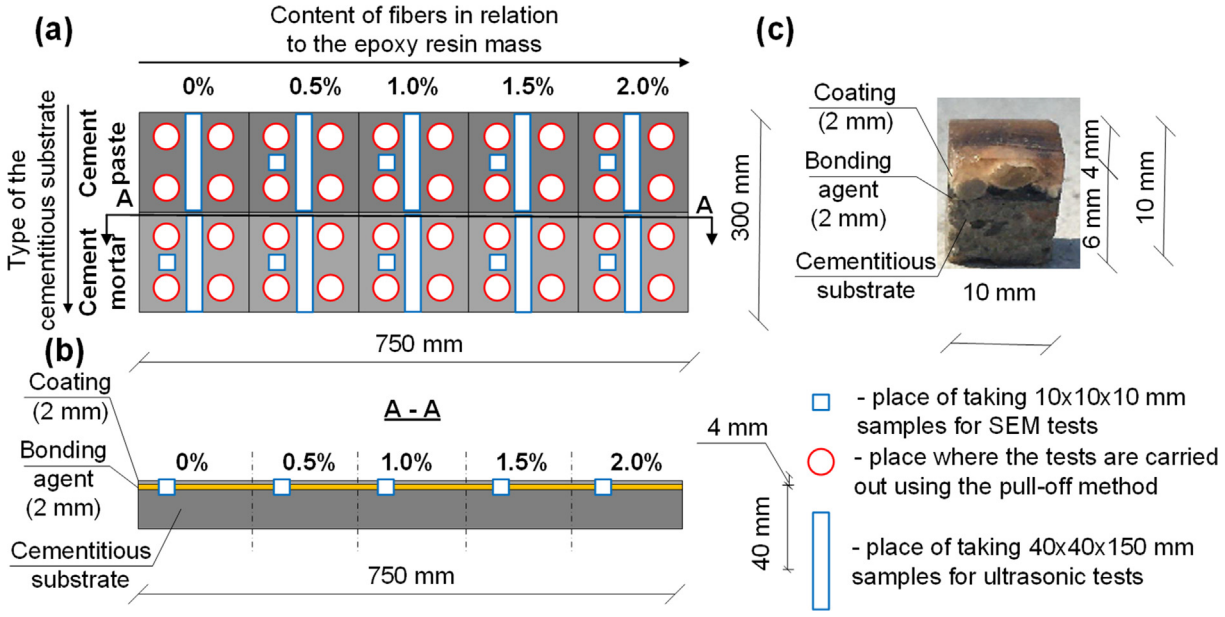

Fig. 3. Specimens: (a) specimen type, (b) cross-section of a specimen, (c) sample specimen for SEM test.

using a pull-off tester made by Proceq (Schwerzenbach, Switzerland). The tester automatically determined the pull-off strength by plotting the time-dependent load increment (Fig. 4**(a)**).

To connect the arm of the pull-off tester and the top layer of the specimen, a steel disc was used (Fig. 4**(b)**). The steel discs were glued to the specimens by using the epoxy resin Epididan 5, together with the hardener Z1 from Ciech Sarzyna (Nowa Sarzyna) in a proportion of 100 to 12. The epoxy resin was applied and carefully spread within the interface between the steel discs and the surface of the bonding agent. After that, any excess resin had to be removed. Once the adhesive was fully cured, the pull-off tests were performed. The maximum time required to obtain failure was 100 s (with a peel rate of 0.05 MPa/s). At least three tests were performed for each sample type (see Fig. 3**(a)**).

3.2. Ultrasonic testing

Ultrasonic pulse velocity measurements were carried out to investigate the degree of resin penetration into the substrate with regard to depth. The tested specimens for the pull-off tests were employed for performing ultrasonic tests. With this aim, each specimen was cut into two parts (see Fig. 3) and the two surfaces were ground so that they were parallel to each other. The ultrasonic

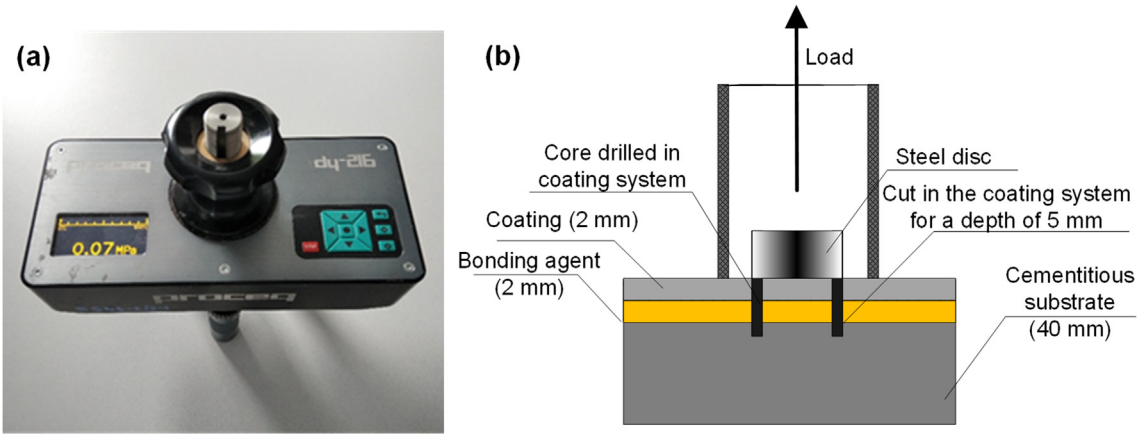

Fig. 4. The pull-off tester made by Proceq (Schwerzenbach, Switzerland):(a) view of the test device, (b) scheme of the testing system.

device made by Proceq (Schwerzenbach, Switzerland) shown in Fig. 5 **(a)** was used.

Measurements of ultrasonic pulse velocity were first performed close to the coating's surface, and then at a depth equal to 2 mm, i.e., at the interface between the bonding agent and the coating. At a depth equal to 4 mm, pores on the resin and cementitious substrates were detected. In the cementitious substrates, the ultrasonic pulse velocity measurements were carried out every 4 mm up to a depth of 20 mm, with a total of 6 measurements being conducted for each tested specimen (Fig. 5**(b)**).

3.3. Microstructural and chemical analysis

A scanning electron microscope JSM-6610A made by JEOL (Tokyo, Japan) with tungsten filament was used to investigate the microstructure of the interphase between the bonding agent and the cementitious substrate. Such analysis was carried out using the BSE mode (material contrast of the backscattered electrons detector). A current of 40nA, an accelerating voltage of 20 kV, and a distance from the sample of 10 mm were applied.

The specimens used for the SEM observations (Fig. 3**(c)**) were embedded in epoxy resin (non-conductive) and ground using sandpapers in the 120–1200-grit range. Finally, their surface was polished using a diamond paste medium (diamond size 6 μm and 1 μm). To obtain the electric conductivity of the specimen, and to avoid electric charging of its cross-section, a conductive track made of copper tape was applied. For this purpose, the whole specimen was covered with a 35 nm thick layer of conductive carbon coating, which was applied in a high vacuum (2×10^{-5} Pa) using the thermal spraying method and graphite electrodes.

The X-ray dispersed energy spectrometer (EDX, EDS) (Tokyo, Japan) with a count rate of about 4000 cps was used to determine the chemical composition of the specimens. The dead time of the detector did not exceed 15%. Quantitative analyses were performed by using both the JEOL software (JEOL JED-2300 Analysis Station) and the integrated ZAF method.

Chemical element mapping, which provides information concerning the elements that characterize the interphase between the bonding agent and the cementitious substrate, had a resolution of 512 × 384 points with a field size of 135 × 100 μm.

3.4. Numerical modelling

Nonlinear three-dimensional finite-element simulations were carried out to capture the adhesive performance of epoxy resin coatings with a novel bonding agent. The finite element method (FEM) simulations were performed using the commercial software ABAQUS version 2017. A nonlinear analysis enabling geometric nonlinearities based on the direct full Newton-Raphson technique was used to run the simulations. To obtain the ultimate pull-off strength preliminary, the ultimate tensile strength of the substrate was studied using inverse analysis to understand the softening behaviour of the substrate during tensile stresses. A Concrete Damage Plasticity (CDP) model was utilized for this purpose. The interaction between different pull-off test components was considered using a predefined cohesive function in ABAQUS. The output results of the FE simulation presented the capability of the proposed model for capturing the ultimate tensile strength during pull-off tests.

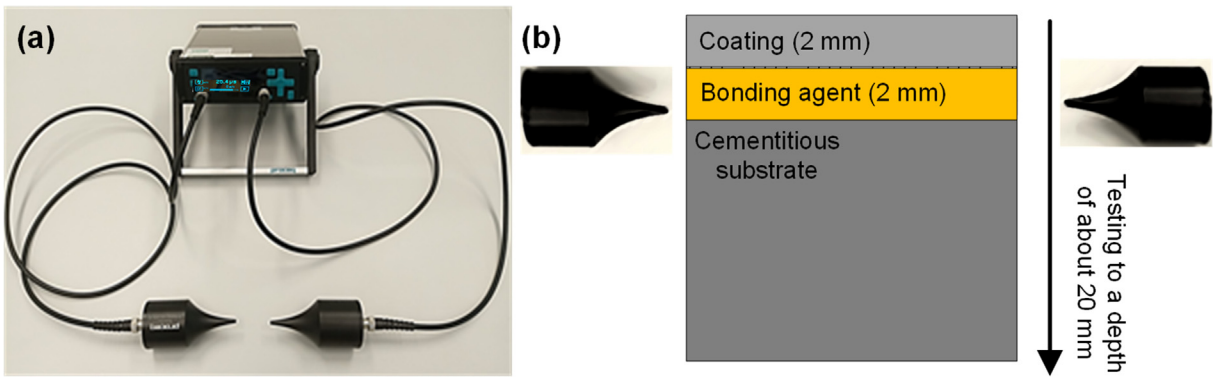

Fig. 5. (a) The ultrasonic device made by Proceq (Schwerzenbach, Switzerland), and (b) the ultrasonic pulse velocity measurement.

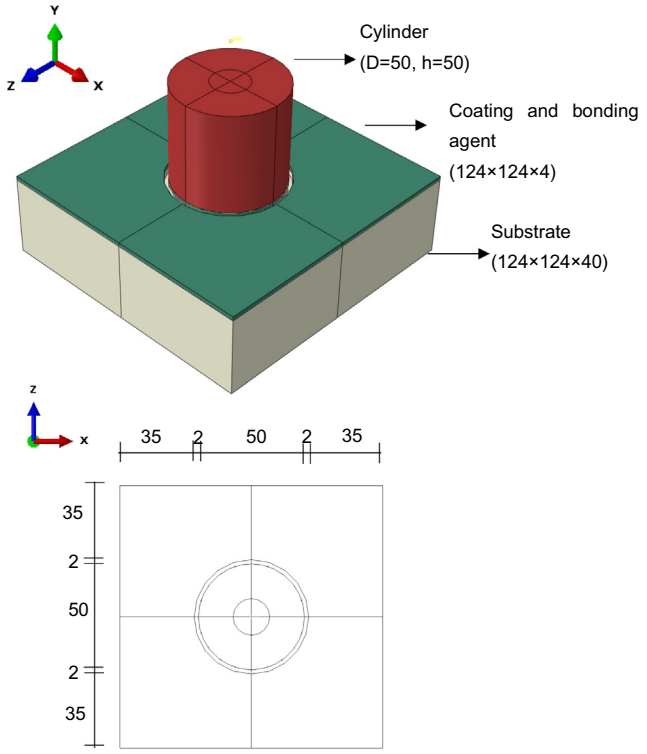

Fig. 6. Geometry and constituents for finite element method (FEM) (all dimensions in mm).

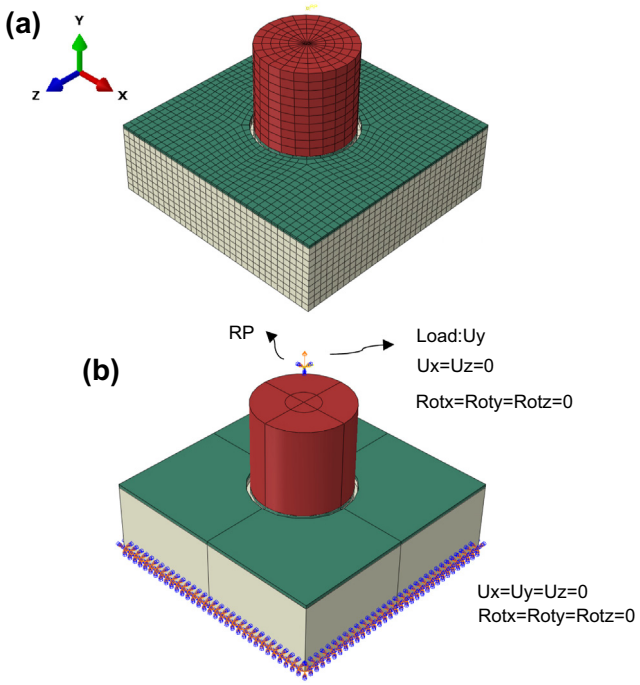

Fig. 7. Finite element (FE) model description: (a) meshing, (b) boundary and loading conditions.

The schematic description of the model geometry and constituents is depicted in Fig. 6. For the FEM analysis, the pull-off test constituents were comprised of steel cylinder for loading purpose, coating, bonding agent, and cementitious substrate. It should be mentioned that, in this stage of research, for some simplification and avoiding the influence of different parameters, the coating and bonding agent were considered as one layer. The cylinder, dimensioned by 50 mm (diameter) and 50 mm (height) and for avoiding the influence of deformation during the analysis, a rigid body was selected with a reference point 5 mm outside in the centerline direction.

Pull-off response in the FE analysis depends mainly on the constituents responses and more specifically due to substrate degradation and interface traction between different layers. Employing a coarse mesh in the area of stress concentration may result in a stiffer response than reality. On the other hand, the extra fine mesh may increase the time of simulation and softer response. After some preliminary analysis, it was found that elements with an approximate 5 mm per side were optimal for the simulation (see Fig. 7**a**). All components were modeled using 3D hexahedral deformable solid elements with eight nodes and three degrees of freedom per node (C3D8).

Since in the experimental part the cementitious substrate was not allowed to move and rotate in any direction and angles, in the numerical simulations all degree freedoms for the displacement (Ux, Uy, and Uz) and all degree freedoms for rotation (Rotx, Roty and Rotz) were considered fixed. Regarding the loading, a reference point (RP) was allocated to the cylinder specimen and the same approach as for the supporting was used except the degree of the displacement in "y" direction was not fixed. The tensile load was applied in the unfixed degree of displacement (Uy) in the RP as a displacement with a maximum 1 mm displacement. The schematic for loading and boundary conditions is depicted in Fig. 7.

ABAQUS/STATIC GENERAL was used for the calculation with a total time 1 s, the maximum number of increments of 10,000, increment size 0.001 for initial and 0.01 for the maximum.

The epoxy resin was defined as an isotropic material with linear- elastic properties. The performed inverse analysis, Young's modulus of 4 GPa, was chosen for this material. Regarding the substrate, the simplified CDP model was used. This model assumes that the cracking starts to initiate at the point where the maximum principal strain is positive and the plastic strain is greater than zero. By using some trial and error, the plasticity parameters for CDP model were selected and tabulated in Table 1.

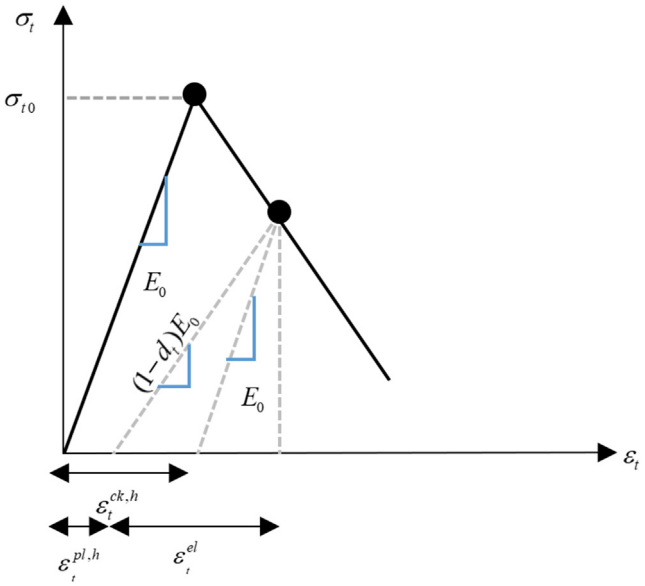

Fig. 8. Response of concrete to a tensile loading condition.

Table 2
Plasticity parameters for concrete damage plasticity (CDP) model.

Dilation angle (φ)	Eccentricity (ε)	$\frac{\sigma_{c0}}{\sigma_{b0}}$	K_c	Viscosity (μ)
31	0.10	0.667	1.16	5×10^{-16}

Table 3
Substrate properties defined during finite element (FE) simulation.

Elastic behaviour			
Density (kg/mm^3) 2.5e-9			
Young's Modulus 36 GPa			
Poission's ratio 0.19			
Plastic behaviour			
Compressive behaviour		Tensile behaviour	
Yeild Stress (MPa)	Inelastic strain (%)	Yeild Stress (MPa)	Inelastic strain (%)
54	0	3.2	0
		2	0. 2
		1.2	0.04
		0.5	0.09

In the simplified CDP, the values of the hardening and softening variables were used for the determination of the cracking and crushing trends, respectively. The damage states in compression and tension were characterized independently by two hardening variables indicated by $\varepsilon_c^{pl,h}$ and $\varepsilon_t^{pl,h}$, which referred to the equivalent plastic strains in compression and tension, respectively [56]. In this study, since the substrate was assumed that the effect of compressive is negligible, the uniaxial compressive behavior was defined as maximum yield stress of 55 MPa and inelastic strain equal to zero. Regarding the tensile behavior, the hardening and softening behavior were defined in Fig. 8, based on the models presented in [57].

In CDP model, the plastic hardening strain in tension ($\varepsilon_t^{pl,h}$) was derived in Fig. 8 as the following equations:

$$\sigma_t = (1 - d_t) \times E_0 \times (\varepsilon_t - \varepsilon_t^{pl,h}) \tag{1}$$

$$\varepsilon_t^{ck,h} = \varepsilon_t - \frac{\sigma_t}{E_0} \tag{2}$$

$$\varepsilon_t^{pl,h} = \varepsilon_t - \frac{\sigma_t}{E_0}\left[\frac{1}{1 - d_t}\right] \tag{3}$$

$$\varepsilon_t^{pl,h} = \varepsilon_t^{ck,h} - \frac{d_t}{(1 - d_t)} \times \frac{\sigma_t}{E_0} \tag{4}$$

Fig. 8 shows that with a further increase in the hardening cracking strain ($\varepsilon_t^{ck,h}$), the tension damage will continue to increase and can be presented by Eq. (5):

$$d_t = 1 - \frac{\sigma_t}{\sigma_{t0}} \tag{5}$$

The selected parameters for representing the tensile behaviour of the substrate are tabulated in Table 2.

Two types of interaction were defined in this research. The first one was related to the interaction between cylinder loading and epoxy resin. To avoid the influence of different parameters on the simulation results, it was assumed preliminary using the perfect bond for interaction. Using this strategy, all debonding was assumed to be occurred due to degradation of the bond between epoxy layer and substrate. See (Table 3.).

The second interaction is related to the bond between expoxy resin and cementitious substrate. This interaction was modelled as cohesive. The generalized cohesive behaviour predefined in ABAQUS was used. This is a surface-bed cohesive behaviour defined by a traction separation law as was demonstrated in Fig. 9, based on the model presented in [58].

The model considers linear elastic behavior of stiffness k until reaching a certain value of interface traction strength (t^0) and surface separation (δ^0). Afterward, the initiation and evolution of damage occur up to the ultimate separation. The elastic behavior of the model is simulated by an elastic constitutive matrix that relates the normal and shear stresses (referred to as traction$t$) to the normal and shear separation across the interface (δ). Thus, the surface separation (δ) is computed by

$$[t] = [k][\delta] \tag{6}$$

where $[t] = [\,t_n \quad t_{s1} \quad t_{s2}\,]^T$ and $[\delta] = [\,\delta_n \quad \delta_{s1} \quad \delta_{s2}\,]^T$ are the stress and displacement components. In the simulation, an uncoupled behavior was assumed between the traction and separation. This means that the stress in the normal direction did not result in a separation in the shearing direction, and the shear stress did not lead to any separation in the normal direction.

Degradation of the bond between two adherent surfaces was simulated with a damage model. Initiation of damage was defined by a stress-based traction separation law, and it was assumed that the failure mode corresponded to an opening according to [59]. No mixed mode was considered for simplicity. Consequently, the

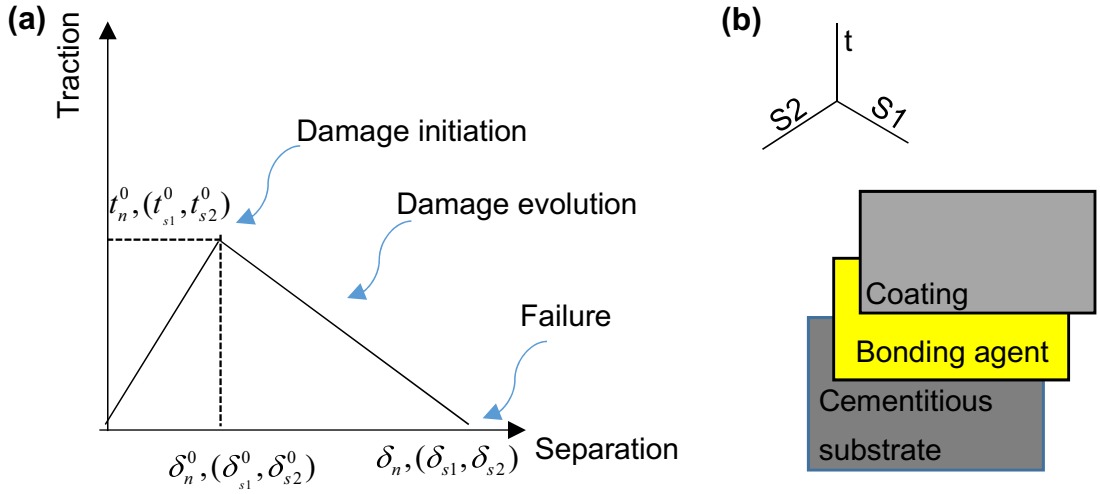

Fig. 9. Cohesive behaviour simulated: (a) traction-separation response, (b) cohesive element.

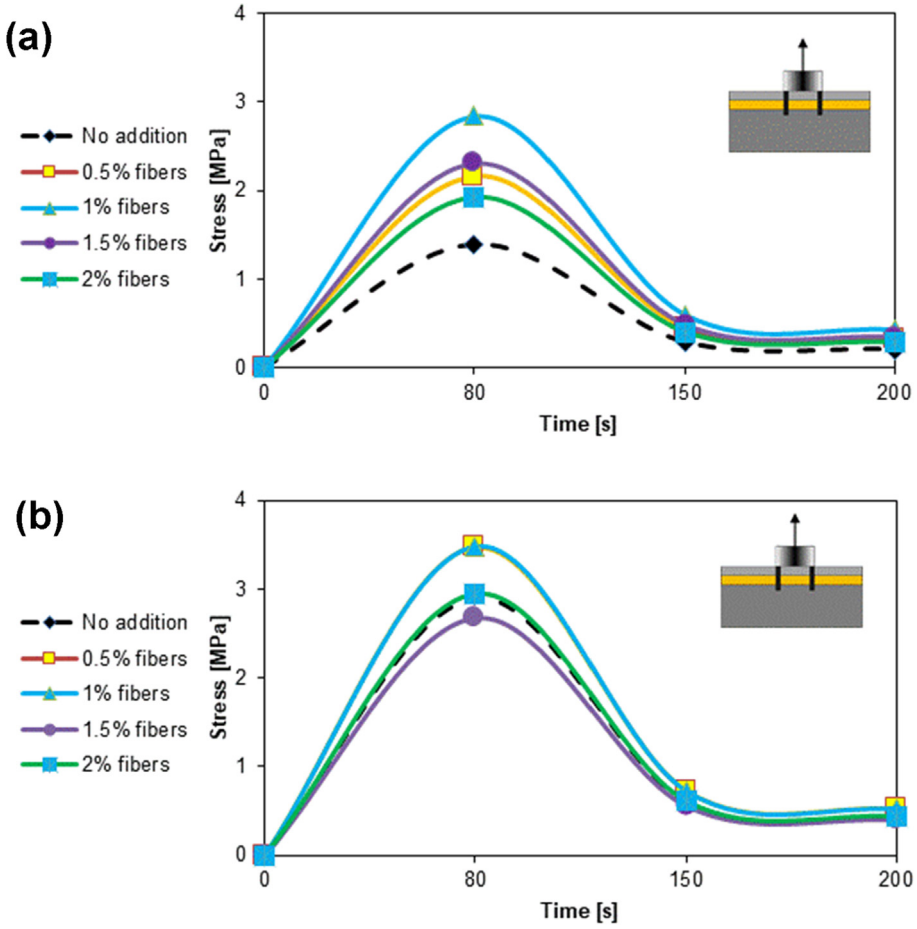

Fig. 10. Average stress with regard to time for the specimens : (a) cement paste substrate, and (b) cement mortar substrate.

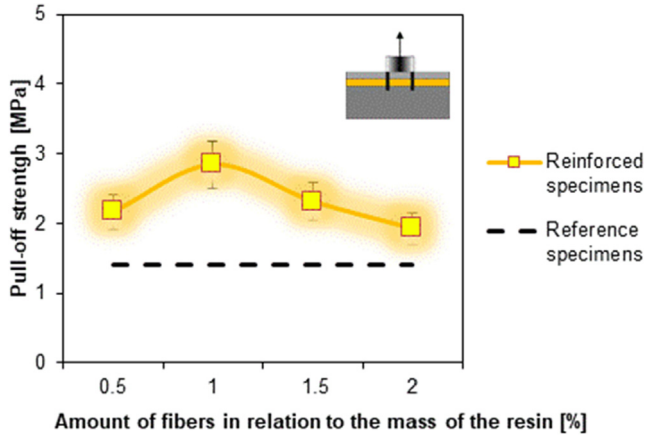

Fig. 11. The pull-off strength between the bonding agent modified with coconut fibers and the cement paste substrate with regard to the content of fibers.

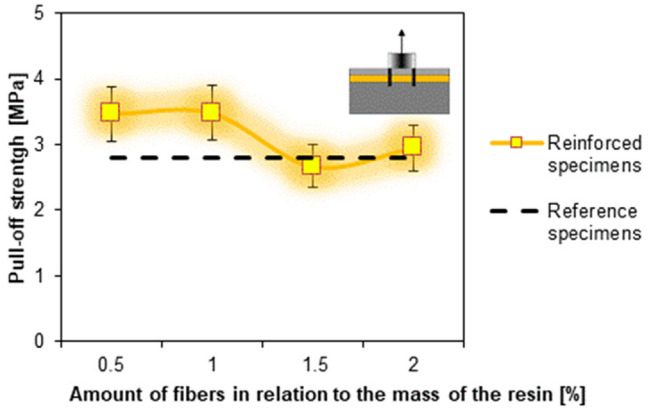

Fig. 12. The pull-off strength between the bonding agent modified with coconut fibers and the cement mortar substrate with regard to the content of fibers.

damage is initiated in the model when the maximum contact stress ratio reaches one of the maximum values [60].

$$\max\left[\frac{\langle t_n\rangle}{t_n^0},\frac{t_{S1}}{t_{S1}^0},\frac{t_{S2}}{t_{S2}^0}\right]=1 \tag{7}$$

where $t_n$is the normal stress, $t_{s1}$and $t_{s2}$are the shear stresses in the planes $s_1$and, $s_2$respectively, and t_n^0,$t_{s1}^0$and $t_{s2}^0$are the peaks of the normal stress and shear stresses respectively (in the planes $s_1$and s_2).

Finally, the inclination of the softening phase in Fig. 9**a** was defined. For the evolution of the initiated damage, an energy-based approach with a linear softening law was used. Fracture energy of 0.01 J was adopted for the simulations.

4. Results

4.1. Pull-off test

It was observed that the specimens were usually damaged as a result of cohesive failure in the substrate. However, a complete detachment of the top layer, due to adhesive failure, was observed in the case of three specimens. In turn, in the case of two specimens, the coating and the bonding agent were only partially ruptured due to cohesive (or adhesive) failure.

The stress-time responses of specimens during the pull-off tests based on the average of the three performed tests are presented in Fig. 10(a) and Fig. 10**(b)** for the cement-based substrate and cement mortar substrate respectively. Inspection of this figure revealed that the trend in all tested specimens were linear until the maximum ultimate load. After this point, due to the degradation of bond strength between substrate and steel cylinder, the specimens can not sustain higher loads and the stiffness was decreased by increasing time. The degradation of stiffness was observed in a smooth trend and in all tested specimens sudden rupture did not observe. In the case of cement paste substrates, the maximum pull-off strength was related to the reinforcement of bonding agents with 1% volume friction of fiber addition. Meanwhile, in the case of cement mortar substrate, the maximum pull-off strength was noticed when the bonding agent was reinforced with the addition of 0.5% and 1% of volume friction of fibers.

Fig. 11 shows the pull-off strength between the bonding agent modified with coconut fibers and the cement paste substrate with regard to the content of fibers. A significant increase in this strength (by 103%) can be observed in the case of the specimen with a 1% content of fibers when compared to the reference value obtained for the specimens without the addition of fibers. It can be noted that the pull-off strength for the reference specimen, equal to 1.4 ± 0.33 MPa, does not satisfy the requirements from the standard EN 1504–2 [63] (usually not less than 1.5 MPa and single results not less than 1.0 MPa). With an increase in the content of the fibers, this value decreases but still remains at a higher level than the reference value.

Fig. 12 shows the pull-off strength between the bonding agent modified with coconut fibers and the cement mortar substrate with regard to the content of fibers. It was observed that when the content of fibers was equal to 0.5% and 1%, the pull-off strength was almost at the same level, equal to 3.47 ± 0.43 MPa and 3.48 ± 0.58 MPa, respectively. In the case when the content of fibers was equal to 1.5%, the pull-off strength turned out to be the lowest (2.67 ± 0.62 MPa). In turn, when the content of fibers was equal to 2%, an increase in the pull-off strength was registered (2.95 ± 0.70 MPa).

It can be summarised that the pull-off strength values obtained in the case of the specimens with the cement mortar substrate, which were modified with vegetable fibers, were greater by about 20% than those obtained in the case of the specimens with the cement paste substrate. It can also be observed that the pull-off strength values for the reference specimens with the mortar substrate are greater by about 50% than those obtained in the case of the specimens with the cement paste substrate. This is an expected and satisfactory result due to the fact that the floors are mainly made of cement mortar, and not cement paste.

The failure pattern of pull-off test of the cement paste substrate is depicted in Fig. 13. The failures can be categorized into two

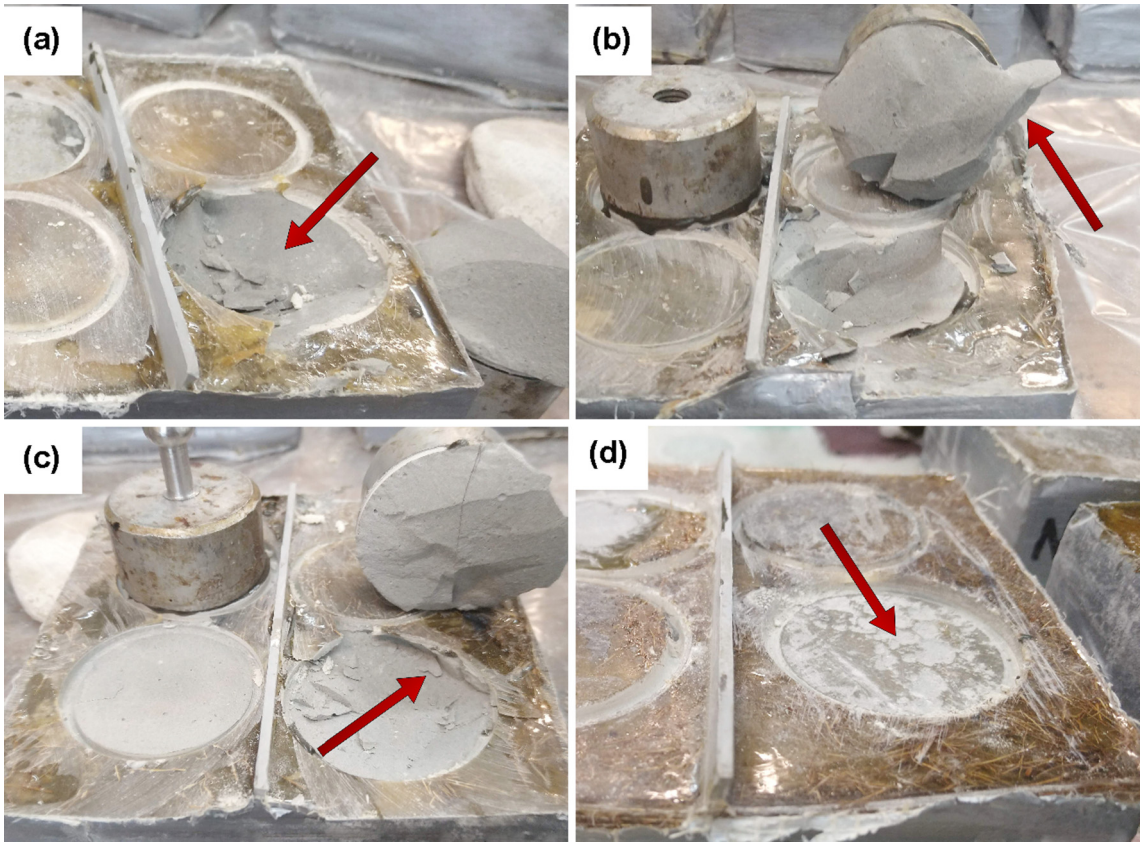

Fig. 13. Selected photos of the surfaces of the fractures of the specimens with the cement paste substrate after the pull-off test: (a) the reference specimen (cohesive failure), (b) the specimen with a 0.5% content of fibers (cohesive failure), (c) the specimen with 1% content of fibers (cohesive failure), and (d) the specimen with a 2% content of fibers (adhesive failure).

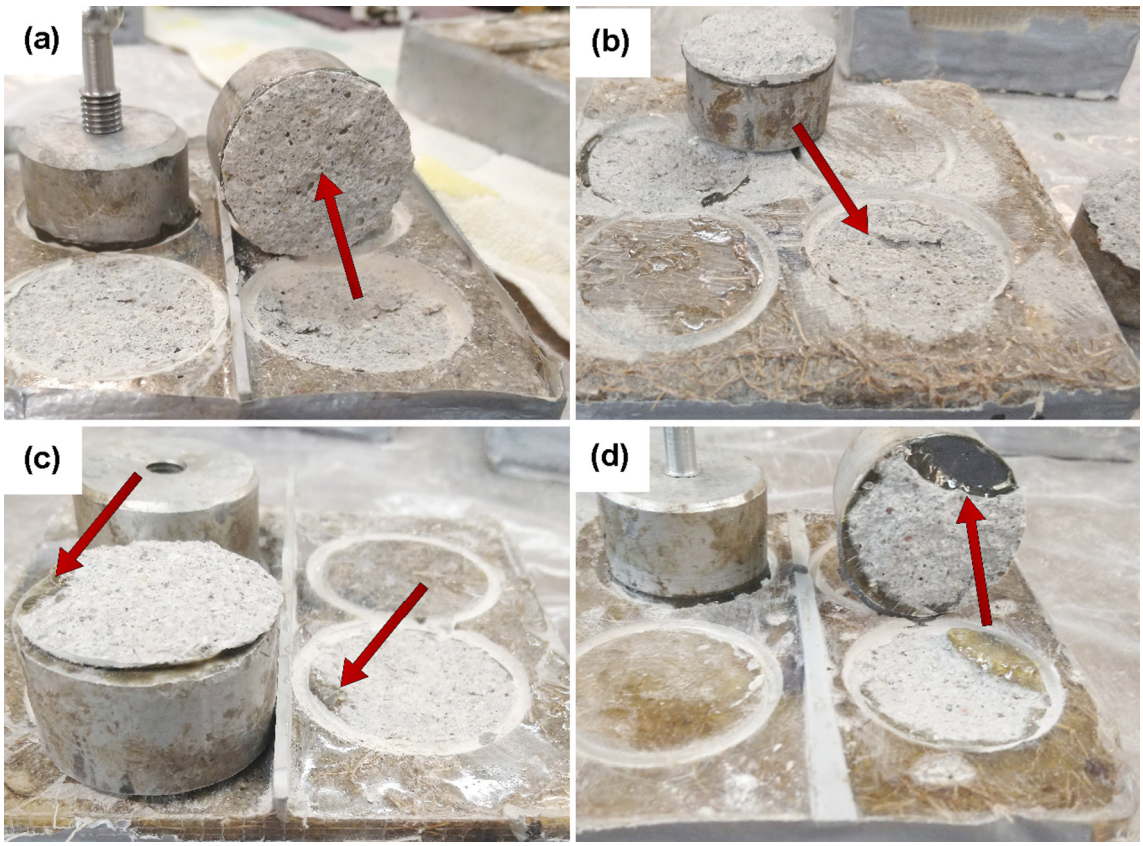

Fig. 14. Selected photos of the surfaces of the fractures of the specimens with the cement mortar substrate after the pull-off test: (a) reference specimens (cohesive failure), (b) specimens with 1.5% content of fibers (cohesive failure), (c) specimens with 0.5% content of fibers (adhesive/cohesive failure), (d) the specimens with a 1% content of fibers (adhesive/cohesive failure).

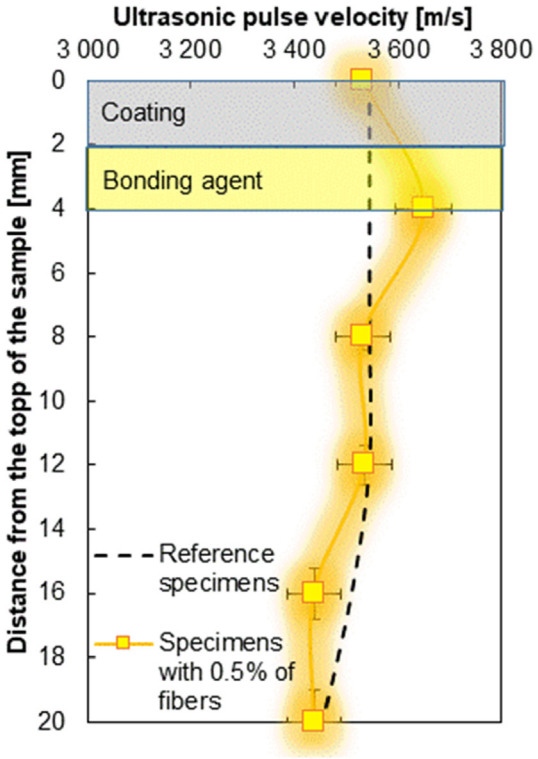

Fig. 15. Ultrasonic pulse velocity vs depth for the specimens with a cement mortar substrate for the reference specimen and specimen containing 0.5% of coconut fiber.

groups : (a) cohesive failure and (b) premature failure. The cohesive failures are depicted in Fig. 13**(a)** and Fig. 13**(b).** It was noticed that in this type of failure, due to the perfect bond between bonding agents, the applied pull-off loads effectively transferred to the substrate. The failure of the substrate occurred when the applied tensile strength was exceeding the ultimate tensile strength of the substrate. From Fig. 13**(a),** it can be seen that a large amount of cement paste, which was broken off inside the specimen and a complete fracture of the specimen occurred during the pulling out of the disc is presented in Fig. 13**(b).** Two kinds of premature failure were noticed. The first one belonged to a partial failure of the resin coating, which was observed in the case of only one specimen (Fig. 13**(c)**). This is probably due to the fact that not enough glue was applied, causing the layers to not bond properly. The second premature failure was related to the detachment of the steel disk from the coating surface, which is depicted in Fig. 13**(d).**

The similar way in the case of cement paste substrate, Fig. 14 shows the selected images of the surfaces of the fractures of the specimens with the cement mortar substrate. Different types of fractures were observed, and they included the rupturing of the substrate (Fig. 14**(a) and (b)**); and partial rupturing of both the coating and the bonding agent. The latter type of rupturing could have been caused by the fact that there was not enough adhesive layer applied (Fig. 14**(c) and (d)**).

4.2. Ultrasonic testing

Due to that the fact the best adhesion performance is obtained for mortar substrates, ultrasonic tests were performed by analysing the epoxy resin coatings on such substrates. The investigations

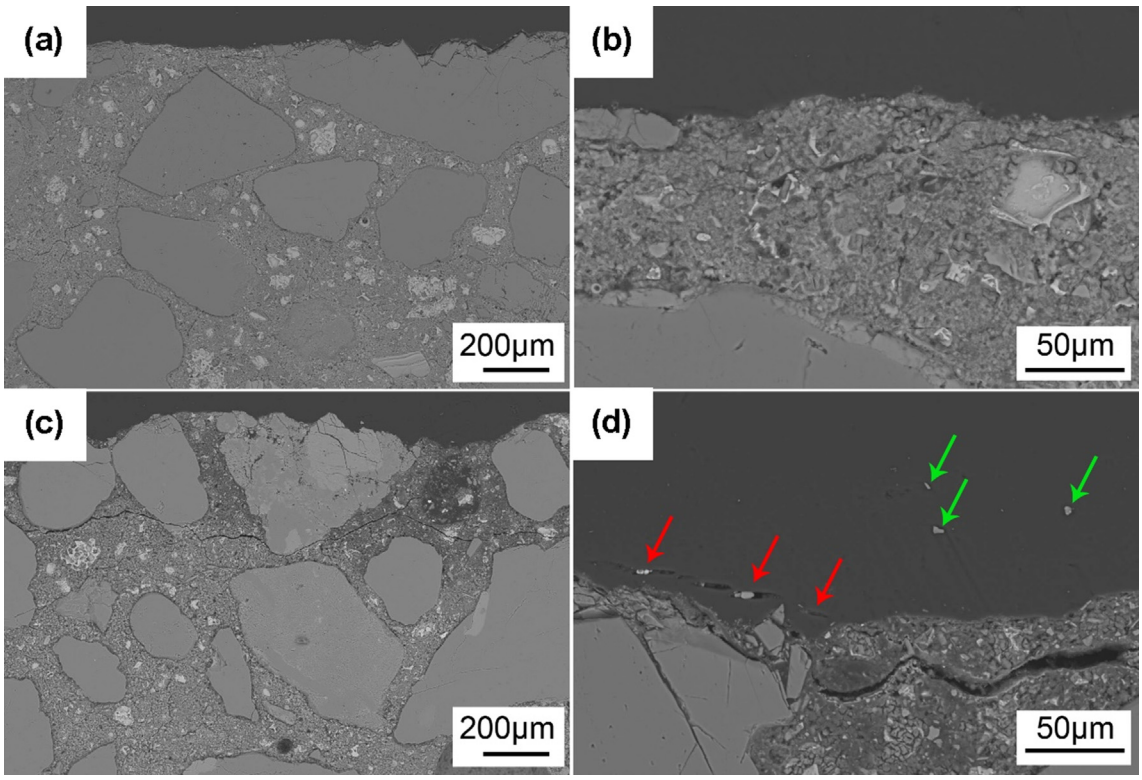

Fig. 16. The microstructure of the interphase between the bonding agent and cement mortar substrate: (a)-(b) the reference specimen and (c)-(d) the specimen containing 0.5% of coconut fiber.

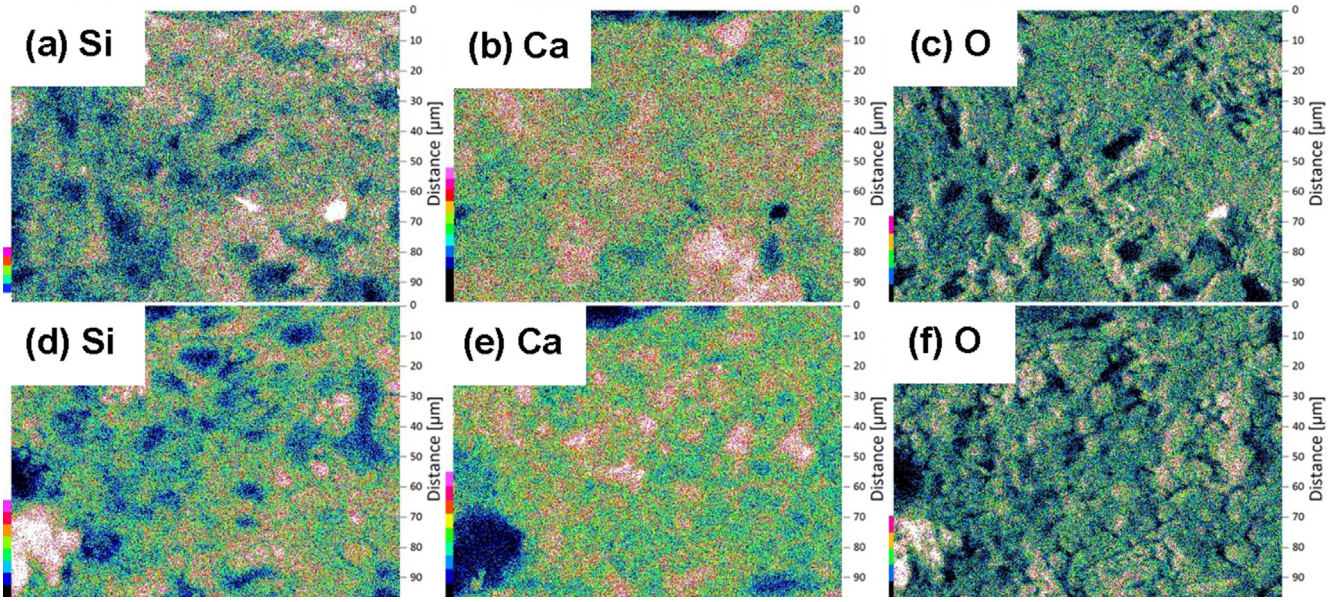

Fig. 17. EDX mapping of the chemical elements (Si, Ca, and O incidence) in the top layer of the mortar substrate for: (a)-(c) the reference specimen, and (d)-(f) the specimen reinforced with fibers.

were carried out on the reference specimen and on the specimen with a 0.5% addition of coconut fibers. The average pull-off strength obtained for the specimens reinforced with 0.5% of coconut fiber is at a similar level compared to those reinforced with 1% of fiber. However, the standard deviation was smaller (0.43 for the specimens reinforced with 0.5% of coconut fiber and 0.58 MPa for the specimens reinforced with 1.0% of coconut fiber).

Fig. 15 shows the ultrasonic pulse velocity with regard to depth. The ultrasonic pulse velocity values in the coating are marked in yellow, the ultrasonic pulse velocity values in the bonding agent are marked in blue, and the ultrasonic pulse velocity values in the cement substrate are marked in green. The measurements were performed at a depth of 20 mm to cover properly the region between the bonding agent and the substrate. This location is the

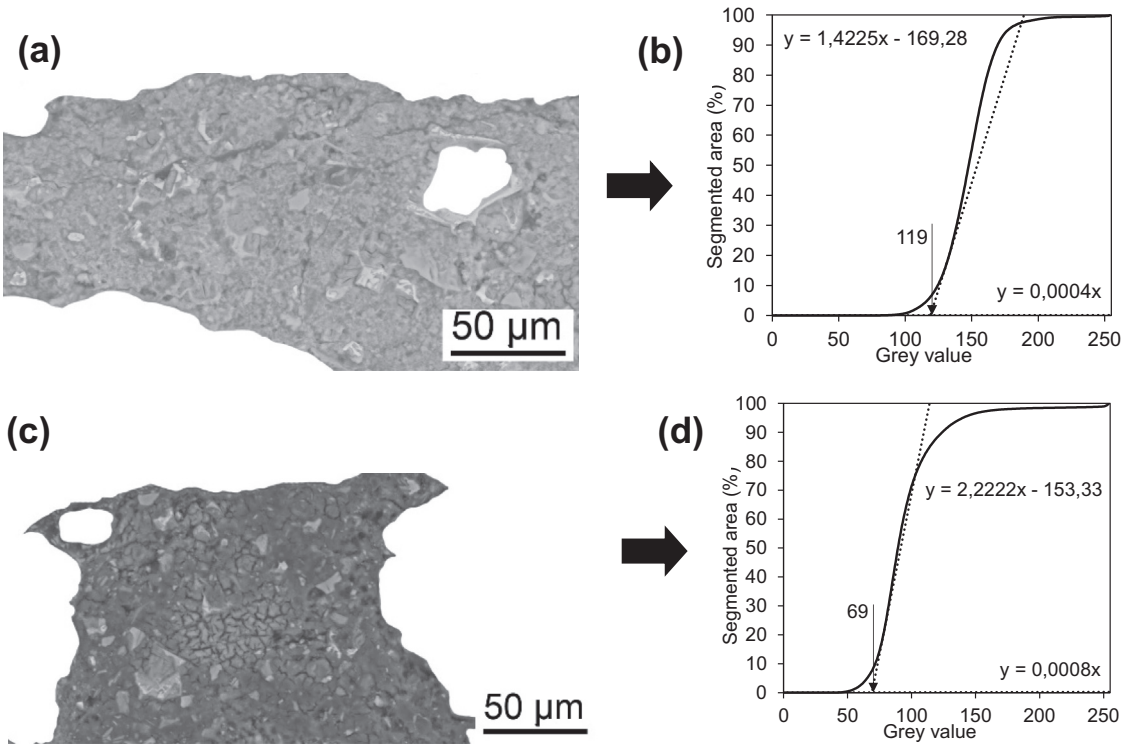

Fig. 18. Representative images of the longitudinal cross-sections of the top layer of the subsurface region of the mortar substrate at x450 magnification, and the cumulative grayscale histograms for: (a), (b) the reference specimen, and (c), (d) the specimen reinforced with 0.5% of coconut fibers.

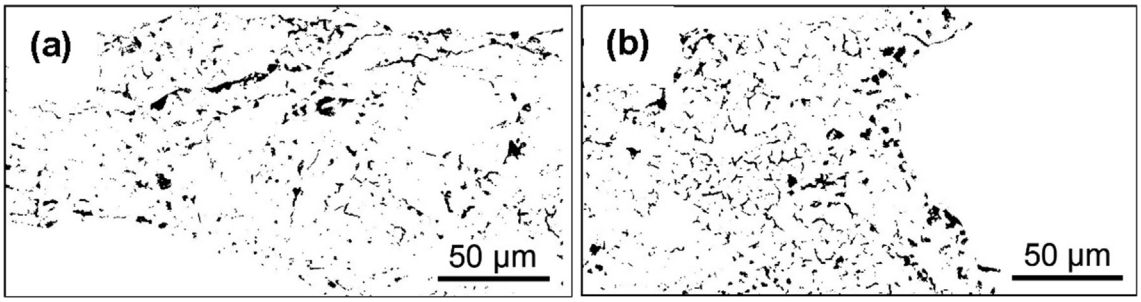

Fig. 19. Images of pores in the form of black pixels obtained at x450 magnification for: (a) the unmodified sample and (b) the sample modified with 0.5% of coconut fiber.

most interesting regarding the aim of the paper, which involves the investigation of the adhesive performance of the novel bonding agent.

For the reference specimen, it can be observed that the ultrasonic pulse velocity in the bonding agent is greater than in the mortar substrate. It is equal to about 3530 ± 36 m/s in the bonding agent and 3400 ± 34 m/s in the substrate. It can also be noted that the ultrasonic pulse velocity at the interface region is similar to that in the bonding agent.

For the reinforced specimen, it can be observed that the ultrasonic pulse velocity in the bonding agent and in the mortar substrate is similar to that for the reference specimen. It can also be noted that the ultrasonic pulse velocity at the interface region is greater than that in the bonding agent. It is equal to about 3630 ± 41 m/s at the interface region, and to 3530 ± 39 m/s in the bonding agent.

4.3. SEM chemical and microstructural analysis

For the same reason as in the case of ultrasonic testing. The SEM tests were performed by analyzing the epoxy resin coatings on mortar substrates on the reference specimen and on the specimen with a 0.5% addition of coconut fiber.

Fig. 16 shows the microstructure of the interphase between the bonding agent and the cement mortar substrate at different magnifications. It can be observed that at a low value of magnification (Fig. 16**(a) and (c)**), the bonding agent completely covers the substrate surface on each specimen. However, at a greater value of magnification (Fig. 16**(b) and (d)**), it is worth noting that local delamination of the bonding agent (see the red arrows) occurred in the reinforced specimen. The delamination is due to the presence of fiber clusters. When the fibers are separated (see the green arrows), such delamination did not occur.

Therefore, it can be concluded that the addition of coconut fibers (up to a certain amount) to an epoxy resin matrix is beneficial with regard to adhesion. In the case when the content of fibers is bigger, the delamination reduces the pull-off strength of the epoxy resin coating. This is due to the increased presence of fiber clusters.

The EDS chemical element distribution was employed to conduct the chemical element mapping of such an interphase. Fig. 17 shows the content of silicon, calcium, and oxygen in the

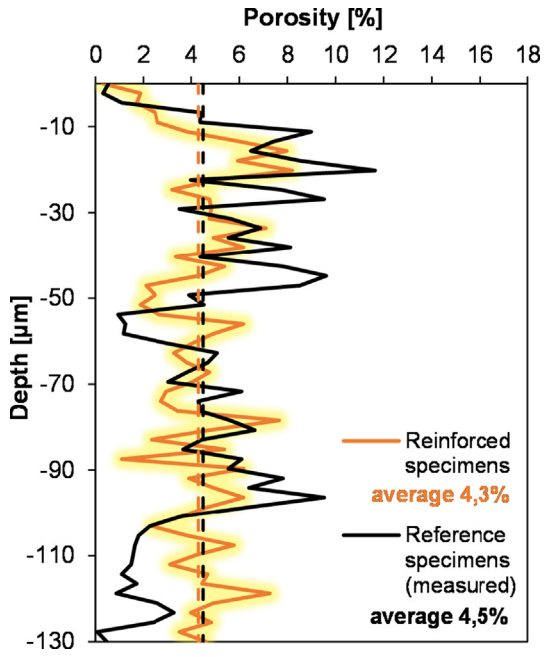

Fig. 20. Graphs of the fractional share of pores along the specimen's depth computed from representative images at x450 magnification.

top layer of the substrate in the cases of the reference specimen (Fig. 17**(a) – (c)**) and the specimen with the addition of coconut fibers (Fig. 17**(d) – (f)**).

The regions of the surfaces that are characterised by a high content of chemical elements were marked with brighter colours. These elements include Si and Ca, which are the main components of the aggregate; and O, which is one of the main components of the cement binder. The regions of the surfaces with a low content of Ca and Si correspond to the occurrence of pores and irregularities, which should be filled with epoxy resin to obtain an adequate pull-off strength of the coating. However, it should be noted that the coconut fibers are too large to be able to penetrate inside the pore structure of the cementitious substrate. The epoxy resin examined in this research mainly consisted of carbon, hydrogen, and oxygen. Carbon and hydrogen quantification cannot be performed because lighter chemical elements than carbon (carbon included) cannot be identified with the use of the EDS method.

Based on the obtained results, a lower oxygen content in the reference specimens (Fig. 17**(c)**) when compared to the specimens reinforced with fibers (Fig. 17**(f)**) can be observed.

Fig. 18 shows the longitudinal cross-sections (in grayscale) of the subsurface region of the mortar substrate (the region just below the interphase between the bonding agent and the substrate) at different degrees of magnification after the manual removal of the aggregates and bonding agent from each image. The cumulative histogram for each such grayscale image was also presented. The grayscale values ranged from 0 (black) to 255 (white) in these figures. The cumulative grayscale histograms were obtained using the ImageJ program. For the analyzed curves, the tangent that corresponded to the inclination of the curve was also determined. The intersection point between the above tangents allowed the so-called "threshold" value to be designated.

All pixels that have a greyscale value between zero and the "threshold" value on the grayscale image are considered as pores. For this evaluation, the ImageJ program was used (Fig. 19). The complete procedure that was used for this purpose is described in Ref. [62].

From the above image, the porosity distribution in the subsurface region of the substrate was computed using the Wolfram Mathematica program (Fig. 20). The depth equal to zero corresponds to the interface between the bonding agent and the substrate. By increasing the depth value, the number of black pixels was summed up and the porosity in percentage was computed. The average porosity of the subsurface region was then calculated and marked with dashed lines in Fig. 20.

From Fig. 20**,** it can be observed that the porosity values were very similar for all examined specimens, 4.5% and 4.3% for the reference and reinforced specimens, respectively. It can be concluded that the addition of 0.5% of coconut fibers did not hinder the penetration of the epoxy resin into the substrate. These results are in agreement with those reported in Ref. [41]**,** in which the effect of polypropylene fibers was similar.

4.4. Numerical modeling

The defined parameters were implemented in the ABAQUS FEM software and the results are described in the following. The maximum pull-off strength was defined as the maximum stress in the normal Y direction (S_y). However, this stress in the local direction is corresponded to the S_{22} sector and is presented in Fig. 21. To understand the distribution of the stress during the test, only half the substrate was depicted in this figure. The figures are tilted by 0% and 0.50%. Those values presented the amount of coconut fiber which was added to the epoxy resin. Moreover, the minimum value of the stress was modified to be equal to zero in all extracted simulations and the maximum one was chosen to be the default.

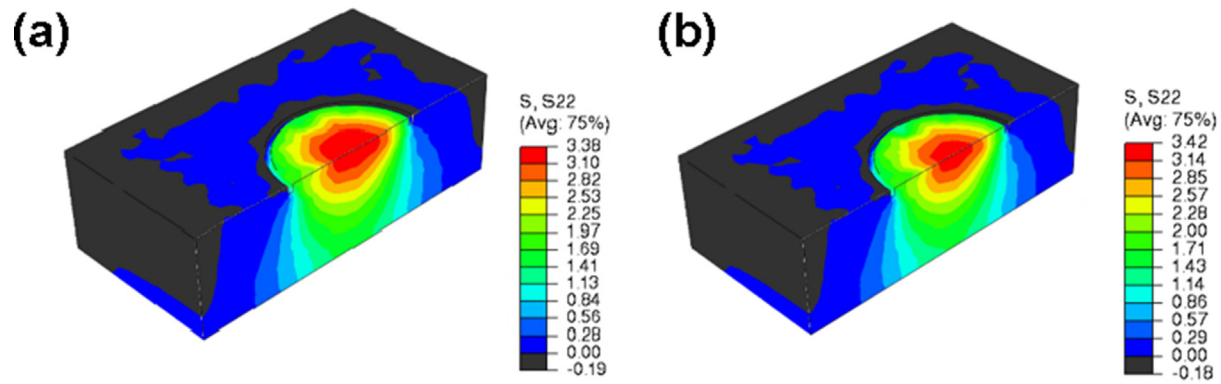

Fig. 21. Numerical modelling of: (a) the unmodified sample, and (b) the sample modified with 0.5% of coconut fiber.

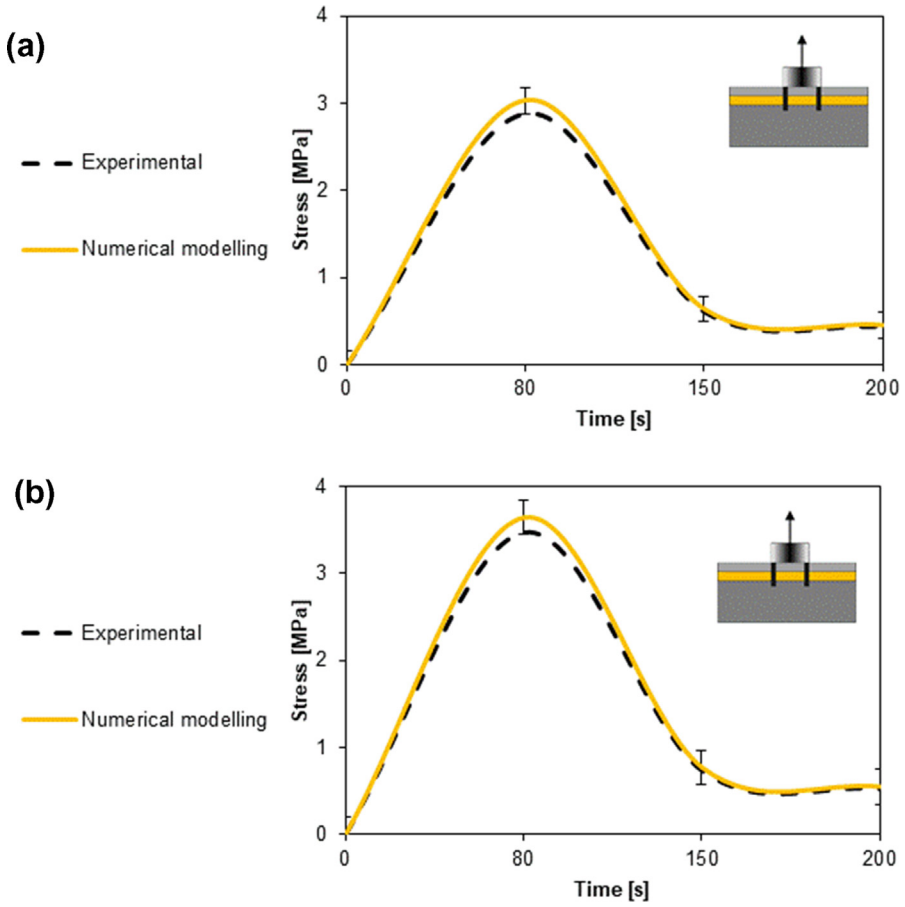

Fig. 22. Experimental and numerical comparison of: (a) the unmodified sample, and (b) the sample modified with 0.5% of coconut fiber.

Using this method, the distribution of the stress is more visible for comparison purposes.

For the unmodified epoxy, the Young's Modulus of 4 GPa was obtained through the inverse analysis. However, in the case of modified epoxy, since adding the fiber is resulted in increasing the stiffness of the material, Young's modulus for 0.5% was obtained by the value of 5.1 GPa.

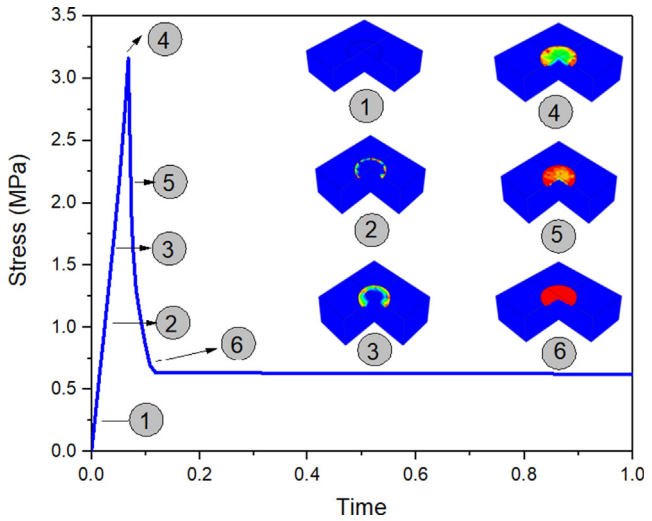

Fig. 23. Pull-off strength versus time for the specimen modified with 0.5% of coconut fiber.

The experimental and predicted numerical pull-off strength are compared in Fig. 22. Inspection of this figure shows the accuracy of the proposed numerical simulation in predicting pull-off strength.

The CDP model was used to present the failure mode during the analysis. It was observed that in all simulated models, the failure happed in the substrate due to the low tensile strength of the substrate. Moreover, the time-dependent failure mode is presented in Fig. 23.

Six stages were observed during the analysis. During stage one, the loading was increased and at the level around 1 MPa of pull-off strength, the substrate started to fail at the exterior part of the cylinder loading (stage 2). By increasing the load, the cracks propagate to the center of the cylinder until during stage 4. After this stage, an inspection of substrate tensile cracks in this stage showed that the specimen can not sustain more loading and the cracks propagate through the thickness of the substrate under the circle of cylinder loading and stage 5 will initiate. In stage 6, the cylinder will be detached from the substrate and that is the end of the experimental loading.

5. Conclusions

In the present paper, a novel epoxy resin bonding agent for improving the bond strength of epoxy resin coating systems was proposed. The matrix of the bonding agent, which was made of epoxy resin, was modified with coconut fibers. Two different types of cementitious substrates were investigated. The following conclusions can be drawn:

In terms of pull-off strength, the optimal content of coconut fibers is 0.5% – 1% of the resin's weight. It was shown that in the

case of the substrate made of cement paste, the optimal value of the content of fibers was 1% of the total weight. Increased content of fibers caused a significant decrease in strength. In the case of the cement mortar substrate, the optimal value of fibers was 1% of the total weight. However, it should be noted that the pull-off strength in the case of the specimens with the addition of 0.5% of coconut fibers was only 0.01 MPa lower than in the case of specimens with the addition of 1% of fiber. In turn, increased content of fibers caused a significant decrease in the pull-off strength of such a modified bonding agent;

The results obtained from the ultrasound tests confirmed that the resin tightly filled the pores located on the surface of the specimens. The high velocity of ultrasound in the upper part of the specimen proved that all surface irregularities were filled with resin. This provided an appropriate balance between the amount of fiber and the viscosity of the resin;

The microstructural SEM analysis showed that epoxy resin with a small addition of fibers is an appropriate compromise between the strength and viscosity of the resin. In such a case, the surface irregularities are tightly filled and the fibers do not form clusters, and therefore the flow of resin on the cement substrate is not affected.

Numerical simulations successfully predicted the pull-off strength using simplified concrete damage plasticity. In all, adherents detachment did not observe and failure was noticed in the substrate due to the low tensile strength of that. The simulations presented that the crack started to initiate at the exterior part of the cylinder loading and propagate to the center of loading.

Funding

This research did not receive any specific grants from funding agencies in the public, commercial, or not-for-profit sectors.

CRediT authorship contribution statement

Łukasz Sadowski: Supervision, Conceptualization, Data curation, Methodology, Writing - original draft, Visualization. **Łukasz Kampa:** Methodology, Resources, Writing - original draft. **Agnieszka Chowaniec:** Data curation, Writing - original draft. **Aleksandra Królicka:** Data curation, Writing - review & editing. **Andrzej Żak:** Supervision, Writing - review & editing. **Hassan Abdoulpour:** Data curation. **Sabrina Vantadori:** Supervision, Writing - review & editing.

Declaration of Competing Interest

The authors declare that they have no known competing financial interests or personal relationships that could have appeared to influence the work reported in this paper.

Acknowledgments

The authors would like to thank the Si-Tech company (Jakubów, Poland) for providing the epoxy resin; Mateusz Moj and Adrian Chajec for providing the ingredients for the cement substrates; and Marlena Rudner and Piotr Szczypta for helping to prepare the resin coatings. Calculations were carried out thanks to Wroclaw Centre for Networking and Supercomputing.

References

[1] J.K. Park, M.O. Kim, The effect of different exposure conditions on the pull-off strength of various epoxy resins, J. Build. Eng. 38 (2021) 102223.
[2] A.A. Almusallam, F.M. Khan, S.U. Dulaijan, O.S.B. Al-Amoudi, Effectiveness of surface coatings in improving concrete durability, Cem. Concr. Compos. 25 (2003) 473–481.
[3] L. Basheer, P.A.M. Basheer, F.R. Montgomery, D.J. Cleland, Assessment of the effectiveness of protective surface treatments, in: International Conference on Bridges and Flyovers, Hyderabad, India, 1991, 22-27.
[4] Q. Xiang, F. Xiao, Applications of epoxy materials in pavement engineering, Constr. Build. Mater. 235 (2020) 117529.
[5] D. Barnat-Hunek, J. Góra, M.K. Widomski, Durability of Hydrophobic/icephobic coatings in protection of lightweight concrete with waste aggregate, Materials. 14 (1) (2021) 101.
[6] R.N. Swamy, S. Tanikawa, An external surface coating to protect concrete and steel from aggressive environments, Mater Struct. 26 (1993) 465–478.
[7] R.N. Swamy, S. Tanikawa, Surface coatings to preserve concrete durability, in: Narayan Swamy R, editor. Corrosion and Corrosion Protection of Steel in Concrete, 1994, 149-165.
[8] R.N. Swamy, A.K. Suryavanshi, S. Tanikawa, Protective ability of an acrylic based surface coating system against chloride and carbonation penetration into concrete, ACI Mater J. 95 (1998) 101–112.
[9] M. Ibrahim, A.S. Al-Gahtani, M. Maslehuddin, Use of surface treatment materials to improve concrete durability, ACI Mater J. I I (1999) 36–40.
[10] L.A. Modesti, A.S. de Vargas, E.L. Schneider, Repairing concrete with epoxy adhesives, Int. J. Adhes. Adhes. 101 (2020) 102645.
[11] P. Gujar, A. Alex, M. Santhanam, P. Ghosh, Evaluation of interfacial strength between hydrating cement paste and epoxy coating, Constr. Build. Mater. 279 (2021) 122511.
[12] X. Han, B. Yuan, B. Tan, X. Hu, S. Chen, Repair of subsurface micro-cracks in rock using resin pre-coating technique, Constr. Build. Mater. 196 (2019) 485–491.
[13] X. Han, W. Liu, Q. Zhang, Y. Chen, X. Hu, Q. Xiao, S. Chen, Effect of resin pre-coating method on repairing subsurface micro-defects in sandstone and granite, Constr. Build. Mater. 264 (2020) 120144.
[14] N. Al Nuaimi, M.G. Sohail, R.A. Hawileh, J.A. Abdalla, K. Douier, Durability of reinforced concrete beams strengthened by galvanized steel mesh-epoxy systems under harsh environmental conditions, Compos. Struct. 249 (2020) 112547.
[15] R. Hsissou, R. Seghiri, Z. Benzekri, M. Hilali, M. Rafik, A. Elharfi, Polymer composite materials: a comprehensive review, Compos. Struct. 113640 (2021).
[16] S.U. Dulaijan, M. Maslehuddin, M.M. Al-Zahrani, E.A. Al-Juraifani, S.A. Alidi, M. Al-Methtel, Performance evaluation of cement-based surface coatings, in: Proceedings of 2000 International Conference, Repair, Rehabilitation and Maintenance of Concrete Structures and Innovations in Design and Construction, Seoul, Korea, September 19–22, 2000, 321-338.
[17] J. Lv, Z. Cao, X. Hu, Effect of biological coating (Crassostrea gigas) on marine concrete: enhanced durability and mechanisms, Constr. Build. Mater. 285 (2021) 122914.
[18] J.B.M. Dassekpo, W. Feng, Y. Li, L. Miao, Z. Dong, J. Ye, Synthesis and characterization of alkali-activated loess and its application as protective coating, Constr. Build. Mater. 282 (2021) 122631.
[19] A.C.L. Chiovatto, A.V.O. de Godoi, E. Zanardi-Lamardo, F.A. Duarte, T.Á. DelValls, C.D.S. Pereira, Í.B. Castro, Effects of substances released from a coal tar-based coating used to protect harbor structures on oysters, Marine Pollutio Bulletin. 166 (2021) 112221.
[20] P.C. Hewlett, Methods of protecting concrete-coatings and linings, in: Dhir RK, Green JW, editors. Proceedings of the International Conference on Protection of Concrete. London: E & FN Spon, 1991, 105-129.
[21] E.N. Júlio, F.A. Branco, V.D. Silva, J.F. Lourenço, Influence of added concrete compressive strength on adhesion to an existing concrete substrate, Build. Environ. 41 (12) (2006) 1934–1939.
[22] X. Yang, Q. Chen, J. Zeng, J.S. Zhang, C.Y. Shaw, A mass transfer model for simulating volatile organic compound emissions from 'wet' coating materials applied to absorptive substrates, Int. J. Heat Mass Transfer. 44 (9) (2001) 1803–1815.
[23] J. Szymanowski, Evaluation of the adhesion between overlays and substrates in concrete floors: literature survey, recent non-destructive and semi-destructive testing methods, and research gaps, Buildings. 9 (9) (2019) 203.
[24] P. Mayer, A. Dmitruk, N. Leja, E. Pakiet, Pull-off strength of fibre-reinforced composite polymer coatings on steel substrate, J. Adhes. 1–19 (2020).
[25] A. Garbacz, L. Courard, B. Bissonnette, A surface engineering approach applicable to concrete repair engineering, Bulletin of the Polish Academy of Sciences, Technical Sciences. 61(1), 2013, 73-84.
[26] X. Wu, F. Yang, G. Lu, X. Zhao, Z. Chen, S. Qian, A breathable and environmentally friendly superhydrophobic coating for anti-condensation applications, Chem. Eng. J. 412 (2021) 128725.
[27] P. Mayer, A. Dmitruk, M. Jóskiewicz, M. Głuch, Pull-off strength of fiber-reinforced composite polymer coatings on aluminum substrate, J. Adhes. 1–17 (2020).
[28] H. Wei, J. Xia, W. Zhou, L. Zhou, G. Hussain, Q. Li, K.K. Ostrikov, Adhesion and cohesion of epoxy-based industrial composite coatings, Compos. Part B: Eng. 193 (2020) 108035.
[29] A. Chowaniec, Ł. Sadowski, A. Żak, The chemical and microstructural analysis of the adhesive properties of epoxy resin coatings modified using waste glass powder, Appl. Surf. Sci. 504 (2020) 144373.
[30] A. Chowaniec, K. Ostrowski, Epoxy resin coatings modified with waste glass powder for sustainable construction, Czasopismo Techniczne. 8 (2018) 99–109.

[31] Y. Hao, F. Liu, H. Shi, E. Han, Z. Wang, The influence of ultra-fine glass fibers on the mechanical and anticorrosion properties of epoxy coatings, Prog. Chem. Org. Nat. Prod. in Organic Coatings. 71 (2) (2011) 188–197.
[32] A. Afshar, S. Jahandari, H. Rasekh, M. Shariati, A. Afshar, A. Shokrgozar, Corrosion resistance evaluation of rebars with various primers and coatings in concrete modified with different additives, Construct. Build. Mater. 262 (2020) 120034.
[33] I. de la Varga, J.F. Muñoz, R.P. Spragg, C.A. Nickel, L. Bohn, A. Fay, B.A. Graybeal, Nanosilica coatings to improve the tensile bond strength of cementitious grouts, Transp. Res. Rec. 2673 (2019) 586–594.
[34] S.A. Morshed, T.J. Young, W.M. Chirdon, Q. Zhang, J. Tatar, Durability of wet lay-up FRP bonded to concrete with nanomodified epoxy adhesives, J. Adhes. 96 (2020) 1–26.
[35] S. Pourhashema, M. Vaezia, A. Rashidib, Investigating the effect of SiO_2-graphene oxide hybrid as inorganic nanofiller on corrosion protection properties of epoxy coatings, Surf. Coat. Technol. 311 (2017) 282–294.
[36] N. Ahn, Effects of diacrylate monomers on the bond strength of polymer concrete to wet substrates, J. Appl. Polym. Sci. 90 (2003) 991–1000.
[37] J. Do, Y. Soh, Performance of polymer-modified self-leveling mortars with high polymer–cement ratio for floor finishing, Cem. Concr. Res. 33 (2003) 1497–1505.
[38] Y. Li, X. Liu, J. Li, Experimental study of retrofitted cracked concrete with FRP and nanomodified epoxy resin, J. Mater. Civ. Engin. 29 (2017) 04016275.
[39] J. van Der Putten, G. de Schutter, K. van Tittelboom, Surface modification as a technique to improve inter-layer bonding strength in 3D printed cementitious materials, RILEM Technical Letters. 4 (2019) 33–38.
[40] S.B. Kim, N.H. Yi, H.D. Phan, J.W. Nam, J.H.J. Kim, Development of aqua epoxy for repair and strengthening of RC structural members in underwater, Constr. Build. Mater. 23 (2009) 3079–3086.
[41] Ł. Kampa, A. Chowaniec, A. Królicka, Ł. Sadowski, The effect of the addition of polypropylene fibers to primer on the pull-off strength of epoxy resin coatings, Materials (2020) 4674.
[42] N. Sgriccia, M.C. Hawley, M. Misra, Characterization of natural fiber surfaces and natural fiber composites, Compos. Part A: Appl. Sci. Manufac. (2008) 1632–1637.
[43] T. Tan, S.F. Santos, H. Savastano, W.O. Soboyejo, Fracture and resistance-curve behavior in hybrid natural fiber and polypropylene fiber reinforced composites, J Mater Sci. 47 (2012) 2864–2874.
[44] W. Nuthong, P. Uawongsuwan, W. Pivsa-Art, H. Hamada, Impact property of flexible epoxy treated natural fiber reinforced PLA composites, Energy Procedia. 839–847 (2013).
[45] N.B. Shawia, M.A. Jabber, A.F. Mamouri, Mechanical and physical properties of natural fiber cement board for building partitions, Phys. Sci. Res. Int. (2014) 49–53.
[46] P. Lertwattanaruk, A. Suntijitto, Properties of natural fiber cement materials containing coconut coir and oil palm fibers for residential building applications, Constr. Build. Mater. 664–669 (2015).
[47] J. Claramunt, L.J. Fernández-Carrasco, H. Ventura, M. Ardanuy, Natural fiber nonwoven reinforced cement composites as sustainable materials for building envelopes, Constr. Build. Mater. 230–239 (2016).
[48] O. Benaimeche, A. Carpinteri, M. Mellas, C. Ronchei, D. Scorza, S. Vantadori, The influence of date palm mesh fibre reinforcement on flexural and fracture behaviour of a cement-based mortar, Compos. Part B: Eng. 152 (2018) 292–299.
[49] O. Benaimeche, N.T. Seghir, Ł. Sadowski, M. Mellas, The utilization of vegetable fibers in cementitious materials, in: I. Choudhury, S. Hashmi (Eds.), Encyclopedia of Renewable and Sustainable Materials 2020, 1st ed., Elsevier, 2019, pp. 1–14.
[50] L. Czarnecki, D. van Gemert, Innovation in construction materials engineering versus sustainable development, Bulletin of the Polish Academy of Sciences: Technical Sciences, 2017, 765-771.
[51] M. Li, Y. Pu, V.M. Thomas, C.G. Yoo, S. Ozcan, Y. Deng, A.J. Ragauskas, Recent advancements of plant-based natural fiber–reinforced composites and their applications, Eng. Compos. Part B (2020) 108254.
[52] H.U. Ahmed, R.H. Faraj, N. Hilal, A.A. Mohammed, A.F.H. Sherwani, Use of recycled fibers in concrete composites: A systematic comprehensive review, Eng. Compos. Part B (2021) 108769.
[53] E. Taban, A. Khavanin, A. Ohadi, A. Putra, A.J. Jafari, M. Faridan, A. Soleimanian, Study on the acoustic characteristics of natural date palm fibres: experimental and theoretical approaches, Build. Environ. 161 (2019) 106274.
[54] P. Sahu, M.K. Gupta, A review on the properties of natural fibres and its bio-composites: effect of alkali treatment. Proceedings of the Institution of Mechanical Engineers, Part L: Journal of Materials: Design and Applications. 234(1), 2020, 198-217.
[55] ASTM D4541-17, Standard test method for pull-off strength of coatings using portable adhesion testers, ASTM International: West Conshohocken, PA, USA, 2017, 06.02 1–6.
[56] M. Hafezolghorani, F. Hejazi, R. Vaghei, M.S.B. Jaafar, K. Karimzade, Simplified damage plasticity model for concrete, Struct. Eng. Int. 27 (1) (2017) 68–78.
[57] J. Lubliner, J. Oliver, S. Oller, E. Oñate, A plastic-damage model for concrete, Int. J. Solids Struct. 25 (3) (1989) 299–326.
[58] H. Abdolpour, J. Garzón-Roca, J.M. Sena-Cruz, J.A. Barros, I.B. Valente, FEM-based numerical strategy for analysis of composite modular floor prototype for emergency housing applications, J. Struct. Eng. 146 (1) (2020) 04019172.
[59] O.L. Bowie, Rectangular tensile sheet with symmetric edge cracks, J. Appl. Mech. 31 (2) (1964) 208–212.
[60] Z.K. Awad, T. Aravinthan, Y. Zhuge, Experimental and numerical analysis of an innovative GFRP sandwich floor panel under point load, Eng. Struct. 41 (2012) 126–135.
[61] C.A. Schneider, W.S. Rasband, K.W. Eliceiri, NIH Image to ImageJ: 25 years of image analysis, Nature Methods. 9 (7) (2012) 671–675.
[62] H.S. Wong, N. Buenfeld, M. Head, Pore segmentation of cement-based materials from backscattered electron images, Cem. Concr. Res. 36 (36) (2006) 1083–1090.
[63] EN 1504-2, Products and systems for the protection and repair of concrete structures. Definitions, requirements, quality control and evaluation of conformity. Surface protection systems for concrete.